CrossMark

Effects of Thermally Sprayed Aluminum Coating on the Corrosion Fatigue Behavior of X80 Steel in 3.5 wt.% NaCl

Weimin Zhao, Timing Zhang, Ruofei Xin, Manman Wang, Hua Ai, Jianbo Sun, and Yong Wang

Corrosion fatigue and fatigue crack propagation experiments were conducted using X80 steel (with and without aluminum coating) in 3.5 wt.% NaCl solution. Results show that the aluminum coating could significantly improve the corrosion fatigue life of the steel substrate, and that this influence would be enhanced by decreasing the applied stress. However, the crack growth rate of the aluminum-coated X80 steel was slightly higher than that of bare X80 steel. Therefore, the presence of aluminum coating extends the crack initiation stage, and the inhibiting effect of aluminum coating on crack initiation outweighs its promotion of crack propagation. The acting mechanisms of the aluminum coating on crack initiation and propagation were discussed.

1. Introduction

Given that the exploration and development of offshore oil and gas resources shift to deep (>500 m) or ultra-deep (>1500 m) waters, the application of long, flexible structures such as subsea pipeline and risers has expanded. For these steel structures, corrosion fatigue is one of the main failure modes under the joint action of cycling loading (Ref 1) and a corrosive environment. Fatigue cracks of high-strength steel in sea water preferentially initiate from corrosion pits (Ref 2, 3) because of the pits' stress concentration effects and irreparable damage caused by corrosion products (Ref 2). Since crack nucleation is facilitated by corrosion, the total life of a material in corrosion fatigue is significantly reduced in comparison with that in mechanical fatigue (Ref 4). Therefore, corrosion fatigue life of high-strength steel can be extended by inhibiting corrosion.

Numerous methods have been used to reduce corrosion, including surface coating by appropriate materials (Ref 5). Zinc and aluminum, as well as their alloys, have been extensively used as steel coatings in the bridge industry, navy, and offshore oil exploration drill platforms. Their sacrificial corrosion protection and relatively low corrosion rates make them suitable for harsh environments (Ref 6). Numerous techniques can be used to pre-

pare anodic coating, such as thermal spraying, hot dipping, and cold spraying, among which, thermal spraying technology is highly developed and can offer high output at low cost. Long-time practical applications (Ref 7, 8) show that thermally sprayed anodic metal coatings could effectively protect marine structures from corrosion. However, the suitability of applying anodic coatings to riser systems, in which corrosion fatigue is the main failure mechanism, needs experimental support.

Anodic metal coatings protect steel substrates by isolation function and cathodic protection. Isolation function uses coatings to prevent the corrosive medium from forming contact with the steel substrate. The protective function increases with the decrease in porosity and increase in self-corrosion resistance. Numerous studies have been conducted to improve the corrosion protection performance of coatings, such as optimizing coating structure (Ref 9, 10), improving the density of coatings, or developing new sealing methods (Ref 11, 12). However, marine structures, such as deep-water risers, are subject to various random loads, which may result in bending stress. Khan et al. (Ref 13) found that maximum bending stress in a steel catenary riser (SCR) caused by random wave can reach 84.93 MPa, which can increase to approximately 300 MPa under random waves and ocean current. Liu et al. (Ref 14) found that the incidence of von Mises stress-induced grounding accidents in deep-water drilling riser under typhoon conditions increases as water depth decreases, and the maximum von Mises stress of risers is 557 MPa at 1030 m water depth. These bending stress induce deformation in steel substrate. Whether the wire-arc sprayed coating can accommodate the maximum deformation or not is uncertain. If the anodic coatings show peeling or cracking, then the coating loses the isolation effect.

When cracks or local peeling appear in the coating, anodic metal coatings can still prevent steel substrate from corrosion by sacrificial anode cathodic protection.

Weimin Zhao, Timing Zhang, Ruofei Xin, Manman Wang, Hua Ai, Jianbo Sun, and **Yong Wang**, College of Mechanical and Electrical Engineering, China University of Petroleum, 66 Changjiang West Road, Qingdao 266580, China. Contact e-mail: zhaowm@upc.edu.cn.

However, cathodic protection can induce a hydrogen evolution reaction, and the absorbed hydrogen atoms would penetrate into the steel substrate and cause hydrogen embrittlement (HE) under extremely low cathodic protection potentials (Ref 15, 16). Figueroa and Robinson (Ref 17) found that re-embrittlement of high-strength steel can occur as a result of the absorption of hydrogen during corrosion of a sacrificial metal coating, and the extent of the re-embrittlement is influenced by both the electrochemical potential of the coating and its barrier properties. Tang (Ref 18) studied the hydrogen permeation behavior of hot-dipped steel in seawater and its effects on the mechanical properties of steel substrate. He found that potentials around coating defects are extremely negative such that hydrogen evolution reaction can easily occur, and the fracture mechanism for steel substrate transfers from ductile fracture to quasi-cleavage fracture. Evidently, HE decreases the resistance of a material to fatigue crack propagation.

In general, aluminum and zinc, as well as their alloys, have been successfully used as long-life anti-corrosion coatings for steel structures. However, these coatings exhibit poor mechanical properties, and the cathodic protection around coating defects may be detrimental to fatigue resistance of steel substrate. Therefore, studies on the effects of anodic coatings on corrosion fatigue behavior of steels are essential for the application of these coatings to marine structures under marine environmental loading. In this study, wire-arc spray technique was used to prepare aluminum coatings on X80 steel, and corrosion fatigue experiments and crack growth rate testing were conducted using bare and coated steel samples in 3.5 wt.% NaCl solution.

2. Materials and Experimental Methods

2.1 Materials

X80 steel plate (18.4 mm thick), with yield strength ($R_{t0.5}$) of 585 MPa and tensile strength (R_m) of 690 MPa, was used in this study (Ref 2).

Aluminum wire with 2 mm diameter and purity higher than 99.7% was used as coating material.

2.2 Corrosion Fatigue Experiment

The dimensions of the test specimens (4 mm thickness) used in corrosion fatigue tests are shown in Fig. 1. The larger end of the specimen (A) was fixed to a stationary platform, and then cyclic stress was applied to the specimen by oscillating at the top of the small end (C) during bending fatigue test. The maximum tension and compression stress σ_{max} (on the surface) are uniform in the shaded area (B) since $\sigma_{max} = -\frac{Z_0 \cdot E \cdot H}{L_0^2}$, where Z_0 is the deflection of the small end of the specimen, E is the elastic module of the steel, H is the thickness of the specimen, and L_0 is the length of wedge area. The stress amplitude σ_{max} is independent of the position along the length of wedge area and the stress is uniform in the shaded area (B) (Ref 2).

The surfaces of the bare steel samples were subsequently ground to Ra of 0.4. Thereafter, the specimens were polished using 5 µm diamond paste, and then successively rinsed and cleaned with deionized water and acetone. To prepare steel specimens for thermal spraying, all surfaces were sandblasted using corundum powder, and then a CMD-AS-1620 arc spray system was used to deposit the aluminum coatings. The arc spray parameters, which were optimized by preliminary tests, are listed in Table 1. Since the residual stress in coating is directly related to the distance from the coating/substrate interface, and there is direct relation between this residual stress and the fatigue life of coated specimen (Ref 19), all of the metal coatings were sprayed to a same thickness of approximately 200 µm in order to make coated steel specimens have same average coating residual stress level.

Corrosion fatigue experiments were conducted on researcher-developed cantilever-bending corrosion fatigue testing machines, which were designed to simulate the reciprocating bending state of drilling riser caused by the action of ocean current and waves. Six experiments were carried out simultaneously, and each experiment was deflection controlled. The strain ε was measured on the surface of steel substrate in shaded zone (see Fig. 1), and the stress was calculated basing on $\sigma = E\varepsilon$. The stress amplitudes were 470 (0.8 $R_{t0.5}$), 333 (0.57 $R_{t0.5}$), and 250 MPa (0.43 $R_{t0.5}$). The tests were performed with three replications. The cyclic frequency was 0.5 Hz. Limited by
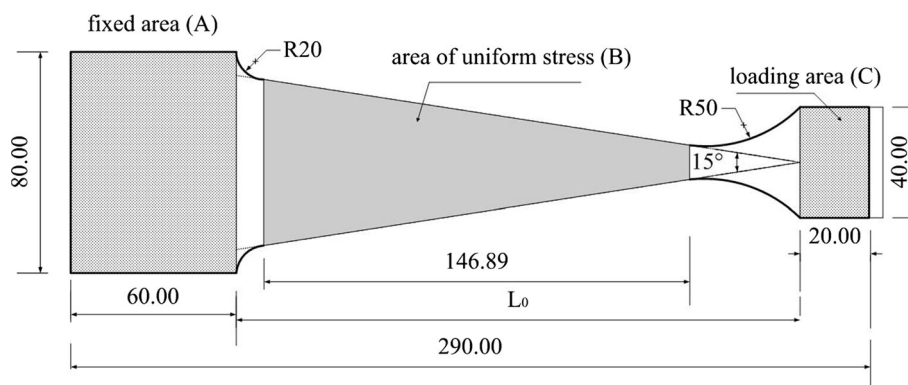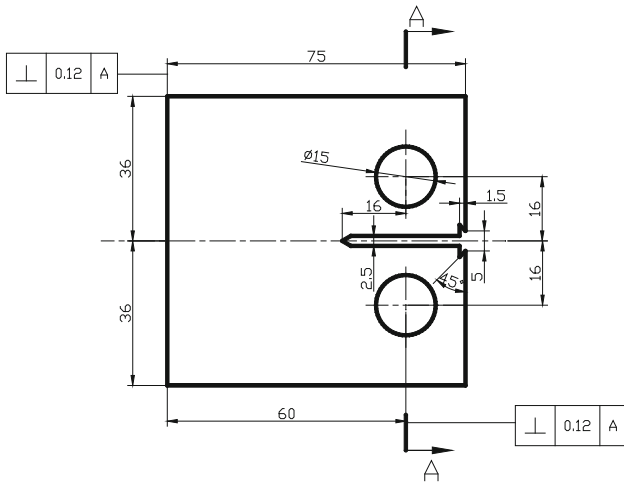

Fig. 1 Size and shape of specimens for corrosion fatigue experiment

Table 1 Arc spray parameters in preparing aluminum coatings

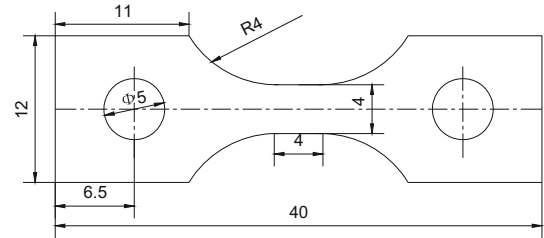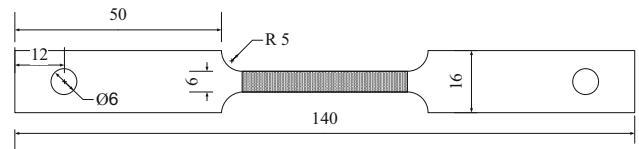| Working pressure, MPa	Spray voltage, V	Spray current, A	Spray distance, mm	Wire feed rate, m/min
0.7	32–33	150	150	7

Fig. 2 Dimensions of CT specimen

Fig. 3 Dimensions of CT specimen for in situ SEM tension

Fig. 4 Schematic of a specimen for SSRT

the design of testing machine, stress ratio (the algebraic ratio of the minimum to maximum stress) cannot be lower than 0, so the stress ratio was set at 0. The specimen was totally immersed in 3.5 wt.% NaCl solution, and the temperature was controlled at 30 ± 1 °C. The corrosion fatigue experiment was conducted until fracture of the specimen, after which, the cross-section of fracture specimen was polished and observed using optical microscopy.

2.3 Corrosion Fatigue Crack Growth Rate Testing

Compact tensile (CT) specimens were used in determining fatigue crack growth rate. The dimensions of these specimens (15 mm thickness) are shown in Fig. 2. All surfaces of bare steel and aluminum-coated specimens were prepared using the same processing procedure as that for preparing the corrosion fatigue specimens. The final polishing direction for the two surfaces of specimens (75 mm × 72 mm) was perpendicular to the direction of crack propagation, so that the length of crack growth can be easily observed.

The experiments to determine the growth rate of fatigue crack were conducted on an MTS 812 computer-controlled servo-hydraulic fatigue testing machine. An initial crack with a length of 2 mm was induced to every specimen in air, in order to eliminate the influence of crack initiation time and decrease measurement error in crack growth rate, and each specimen was loaded under a sinusoidal waveform. After fatigue pre-cracking, the fatigue crack growth rate measurements for bare X80 steel and aluminum-coated steel were conducted in air and also in 3.5 wt.% NaCl solution. The maximum load was 13 kN, the stress ratio was 0.1. The load frequency in air was 10 Hz, and in brine was 0.5 Hz. The length of the fatigue

crack was determined using compliance method with the aid of visual observation.

2.4 In Situ SEM Observation of Coated Steel Failure Process

In situ SEM tension was used to observe the deformation of coated specimen, in order to understand the development of cracking and delamination in coating during tensile test.

The dimensions of these specimens (0.8 mm thickness) are shown in Fig. 3. All surfaces of specimens were ground and polished, and the two sides in gauge length were etched using saturated NaCl solution. A A10-570 SEM was used to observe the etched side during tensile process. The strain state was controlled at 1×10^{-6} s^{-1}.

2.5 Slow Strain Rate Test

Slow strain rate tests (SSRT) were performed to clarify the acting mechanism of aluminum coating on crack propagation of X80 steel substrate.

The dimensions of the X80 steel specimen (2 mm thickness) are shown in Fig. 4. Aluminum-coated steel specimens with 200 μm coating thickness were also prepared. All surfaces of bare steel and aluminum-coated specimens were ground and polished using the same processing procedure as that for preparing the corrosion fatigue specimens.

The SSRTs of bare steel and aluminum-coated steel were conducted under 1×10^{-4} s^{-1} strain rate at room temperature in 3.5 wt.% NaCl solution. In the solution, X80 steel was stretched under self-corrosion potential (−650 mV) and −1000 mV versus saturated calomel

electrode (corresponding to the self-corrosion potential of aluminum-coated steel, achieved by impressed current polarization).

3. Results

3.1 Corrosion Fatigue Behavior

General corrosion occurred on bare X80 steel almost immediately after corrosion fatigue started, and yellowish-brown corrosion products appeared on the surface of the steel specimen. Higher stress amplitude resulted in faster appearance of corrosion products. Three fractured bare steel specimens that were tested under 333 MPa are shown in Fig. 5, after corrosion product removal. We can see that fractures randomly occurred in the uniform applied stress zone (corresponding to zone B in Fig. 1).

During fatigue testing, a camera was used to obtain pictures of coatings through the corrosive medium. Small gas bubbles appeared on the aluminum coating surface after around 2 h of immersion (see small dark gray spots in Fig. 6a). The volume and quantity of bubbles initially

increased and then decreased with time, and gas evolution could be neglected after one week. The gas in bubbles was speculated to be hydrogen, which was produced by self-corrosion of aluminum coating. Small cracks would appear on the coating surface if the applied stress amplitudes are 470 and 333 MPa (see small cracks in Fig. 6b). This finding was due to the coating undergoing deformation with the steel substrate, and the deformation exceeds the deformation ability of coating at high levels of stress. With the increase in time, yellowish-brown corrosion products of the steel substrate appeared along the porosities/cracks in the coating. The covered area of corrosion products expanded with time. Almost the entire coating surface was covered with corrosion products of the steel substrate, but the aluminum coating remained intact on the surface of steel substrate after the tests at 470 and 333 MPa stress amplitudes. No cracks were found in the aluminum coating at 250 MPa, but the aluminum coating was almost used up because of the prolonged testing time.

Table 2 shows the number of cycles to corrosion fatigue failure for bare X80 steel and aluminum-coated X80 steel in 3.5 wt.% NaCl solution under different stress amplitudes. Each cycle number is given as:

$$N = \bar{N} \pm E, \tag{Eq 1}$$

where $\bar{N}$ is the average of each specimen set (three replications), E is the standard error for a 95% confidence interval. The effects of aluminum coating on the corrosion

Fig. 5 Fractured corrosion fatigue test specimens of bare X80 steel under 333 MPa

Table 2 Number of cycles to corrosion fatigue failure and the corresponding relative fatigue life

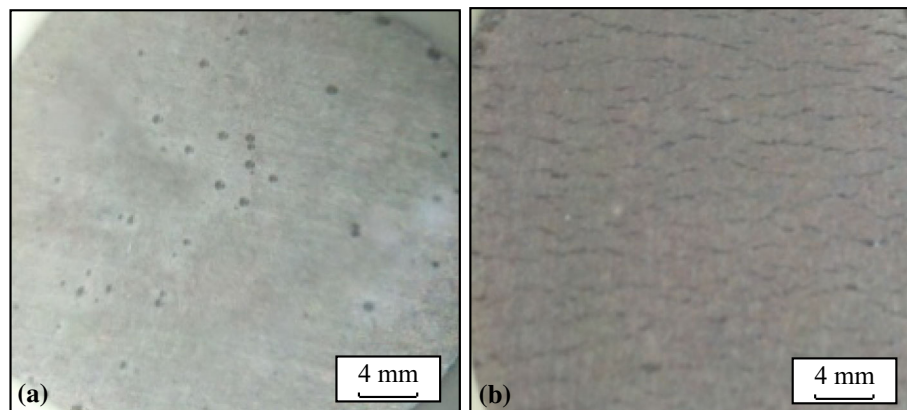| Stress amplitude, MPa	Number of cycles, 10^5		Relative fatigue life
	Bare X80	Al-coated X80	
470	8.37134 ± 0.50650	28.1727 ± 6.6431	3.36
333	17.1033 ± 2.9722	60.2225 ± 15.8249	3.52
250	25.1022 ± 4.8672	138.423 ± 44.939	5.51

Fig. 6 In situ observation of aluminum coatings in corrosion solution during corrosion fatigue test. (a) Gas bubbles; (b) Cracks
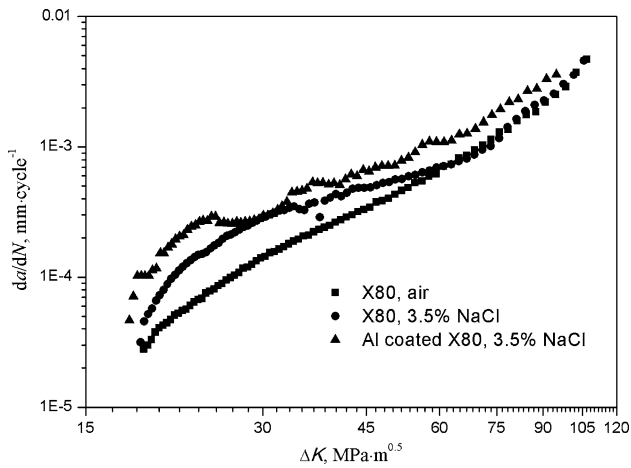
Fig. 7 Relationship between crack growth rate da/dN and stress intensity factor ΔK
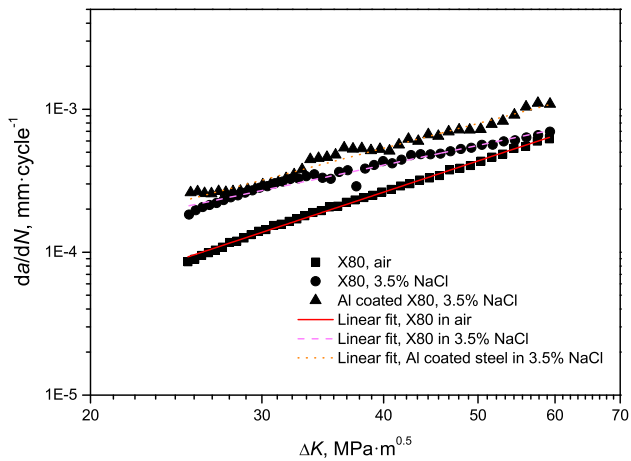

Fig. 8 Fitting diagram of crack growth

fatigue lifespan of X80 steel were evaluated using the "relative fatigue life", which is defined as:

$$\text{Relative fatigue life} = N_C/N_B, \qquad (Eq\ 2)$$

where N_C is the average fatigue life of aluminum-coated X80 specimen set, and N_B is that of bare X80 specimen set.

As shown in Table 2, under all of the tested stress amplitudes, the number of cycles to corrosion fatigue failure for X80 steel was increased by applying aluminum coating. Lower stress amplitude translated to higher relative fatigue life.

3.2 Corrosion Fatigue Crack Growth Rate

The $da/dN - \Delta K$ curves for X80 steel in air, as well as for X80 steel and aluminum-coated X80 steel in 3.5 wt.% NaCl solution, are shown in Fig. 7. In any case, the crack

growth rate increases with the increase in stress intensity factor (ΔK). In general, the crack growth rate for aluminum-coated steel is the highest among the three cases, followed by the growth rate for X80 in solution, and that for X80 in air. By comparing the two curves for bare X80 steel in air and in solution, we can see that the presence of solution can accelerate the rate of crack propagation. The impact of solution on crack growth rate gradually weakens in the intermediate stage, and this impact can be neglected in the final stage of rapid crack propagation. However, the crack growth rate for aluminum-coated X80 steel remained high during the entire crack propagation process.

Paris expression is widely used to determine the fatigue crack growth rate in the intermediate stage (ΔK from about 25 to 60 MPa m$^{0.5}$), in which the crack growth rate increases relatively slowly (Ref [20]):

$$\frac{da}{dN} = C \cdot (\Delta K)^m, \qquad (Eq\ 3)$$

where a is the length of crack propagation, N is the number of loading cycles, da/dN is the crack growth rate, and C or m are material constants related to environmental factors such as temperature, moisture, loading frequency, and the chemical composition of the solution. Equation 3 can be converted into:

$$\lg\left(\frac{da}{dN}\right) = \lg C + m \lg \Delta K \qquad (Eq\ 4)$$

A linear fit can then be made for the intermediate stage of $da/dN - \Delta K$ curves (see Fig. 8), and the slope of the fit line is m. For X80 steel in air, m is 2.25345; For X80 steel in 3.5% NaCl, m is 1.42281; For Al-coated X80 steel in 3.5% NaCl, m is 1.78877. We can see that although the aluminum coating can accelerate the crack growth of the steel substrate at any given ΔK, the coating reduces the difference of m value between X80 steel in air and in 3.5% NaCl. Thus, the aluminum coating may have two different functions on crack growth. First, aluminum coating could inhibit the corrosion of steel, which causes the similarity in the changes in the crack growth rates of the aluminum-coated steel with that of the X80 steel in air. Second, aluminum corrosion can cause local hydrogen permeation, which may change the mechanical properties of steel at the crack tip and induce high crack growth rate.

4. Discussion

Based on the results of corrosion fatigue and crack propagation experiments, aluminum coating could significantly improve the corrosion fatigue life of steel substrate but accelerate its crack growth. Evidently, aluminum coating extends the crack initiation stage, and the inhibiting effect of aluminum coating on crack initiation outweighs its promotion of crack propagation. The acting mechanism of the aluminum coating is described below.
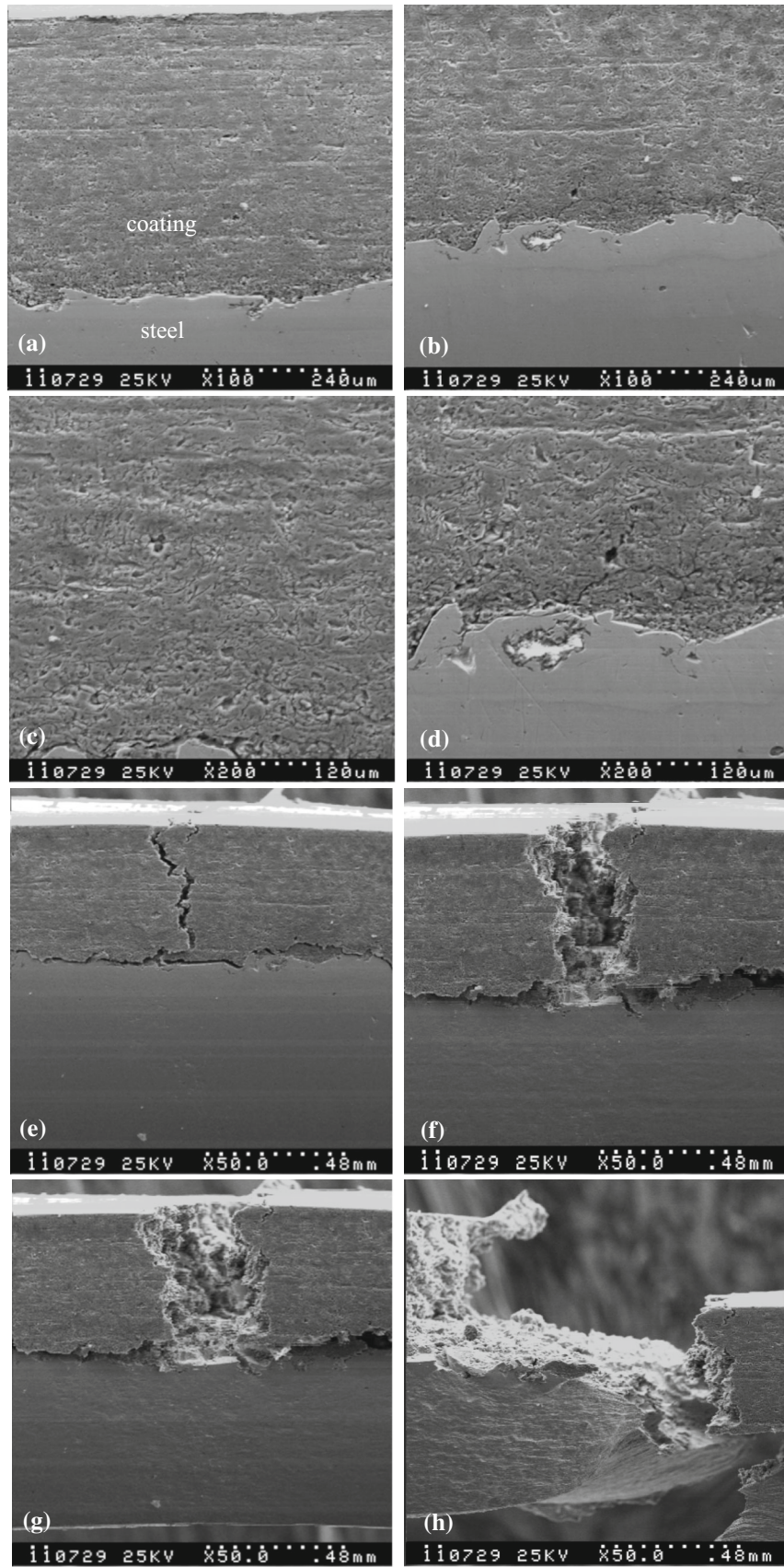
◀**Fig. 9** SEM observation results of aluminum-coated X80 steel during dynamic tensile process. (a) With stress free; (b), (c), and (d) In small amount of elastic deformation; (e) and (f) In large amount of elastic deformation; (g) and (h) In plastic deformation

4.1 Mechanism of Inhibiting Crack Initiation

The influences of aluminum coating on the corrosion fatigue crack initiation in steel substrate can be attributed to three reasons: (1) aluminum coating can mechanically prevent contact between steel substrate and solution, similar to organic coating; (2) thermal spraying can introduce residual compressive stresses in the surface layer of steel substrate; and (3) the aluminum coating provides cathodic protection function when solution penetrates through the coating or some parts of the coating are destroyed.

4.1.1 Mechanical Barrier Effect. By applying SEM to in situ observe the dynamic failure process of aluminum-coated X80 steel during tensile test, the authors found that the bearing capacity of coated steel was determined by steel substrate, and deformation of steel affected the failure process of the coating (see Fig. 9). Aluminum coating undergoes deformation with the steel substrate. Based on the mechanical properties of X80 steel, the failure process of coated steel can be divided into four stages: original state with stress free (Fig. 9a), small amount of elastic deformation (Fig. 9b-d), large amount of elastic deformation (Fig. 9e-f), and plastic deformation (Fig. 9g-h). From Fig. 9(a) to (h), the deformation of steel substrate increases one by one. Compared with original coating, no obvious change can be observed in the microstructure of coating with small amount of elastic deformation (Fig. 9b-c). As the deformation of steel substrate continues to increase, cracks appear in coating at the interface between coating and steel substrate (Fig. 9d, calculated stress higher than 170 MPa). When the stress is higher than 330 MPa, penetrating cracks appear in coating (Fig. 9e). The appearing of penetrating cracks releases stress, therefore cracks' number does not increase, coating remains on the surface of steel substrate, and the distance between crack surface increases with the increase of steel substrate deformation (Fig. 9f-h).

With the applied stress at 470 and 333 MPa, the steel substrate would undergo some deformation which exceeds the deformation ability of coating, and penetrating cracks were formed in the aluminum coating (Fig. 6b). Thus, the mechanical barrier effect was rapidly lost and then the corrosive solution could easily penetrate along cracks into the coating. With the applied stress at 250 MPa, steel substrate only underwent small amount of elastic deformation; no penetrating cracks in coating brought good mechanical barrier effect and low consumption rate. Therefore, the relative fatigue life of the aluminum coating at 470 and 333 MPa stress amplitudes is lower than that at 250 MPa (Table 2).

4.1.2 Stress Level in Steel Surface Layer. Blasting preprocessing can introduce residual compressive stress and yield severe plastic deformation that roughens the surface and produces significant subsurface grain refine-

ment and work hardening (Ref 21). Thermal spraying also introduces compressive stresses in the surface layer of steel substrate (Ref 19). These residual compressive stresses would counteract part of applied tensile stress caused by reverse bending, thus decrease the total stress level in surface layer of steel substrate under aluminum coating. In contrast, there is no residual compressive stress in bare steel, and the total stress level in surface layer is higher than that of coated steel surface.

The total stresses in surface layer of steel substrate would not be higher than the applied stress amplitudes. Since the applied stress amplitudes (470, 333, and 250 MPa) were lower than the yield strength of X80 steel ($R_{t0.5}$, 585 MPa), the steel surfaces were under elastic deformation state during corrosion fatigue testing. The change in electrode potential induced by elastic deformation can be calculated by the following equation (Ref 22):

$$\Delta\phi_H = -\frac{V\Delta P}{zF}, \tag{Eq 5}$$

where V is the molar volume of electrode material, ΔP is the applied load, z is the valence of metal ions, and F is the Faraday constant. It is obvious that the decreasing of electrode potential is directly proportional to stress level. Therefore, comparatively lower total stress level decreases the corrosion tendency of steel surface layer under aluminum coating. Besides, low stress intensity also inhibits fatigue crack initiation.

4.1.3 Cathodic Protection. Cathodic protection from aluminum coating mainly inhibits the corrosion of steel substrate surface. Because we are concerned with this effect on fatigue crack initiation in steel substrate, the remaining aluminum coating was removed from coated specimen after corrosion fatigue testing. Figure 10 shows the corrosion morphology of bare X80 steel and aluminum-coated steel at an applied load of 333 MPa. Overall, aluminum coating could dramatically decrease the number of corrosion pits, see Fig. 10(a) and (b). All the fatigue cracks in bare steel or in aluminum-coated steel initiate from corrosion pits, see Fig. 10(c) and (d), and corrosion pits in coated steel form in sandblast particle imprints (blasting imprint is much bigger than corrosion pit, and corrosion pit has higher ratio of depth to width).

Corrosion fatigue crack initiation of bare X80 steel is due to the stress concentration effects of the corrosion pits and the adhering corrosion products (Ref 2). The anodic aluminum coating can inhibit corrosion and the presence of corrosion pit, and thus, the crack initiation stage of aluminum-coated steel has been remarkably prolonged. However, sandblast particle imprints under the coating provide another crack initiation zone after the corrosive medium had penetrated through cracks or porosities in aluminum coating to the coating-steel interface. A high roughness and the presence of embedded particles enhance crack initiation (Ref 23). Many authors found that grit blasting and coating of the substrate gave rise to a significant decrease in fatigue properties (Ref 24, 25). Meanwhile, blasting also improves the susceptibility to pit
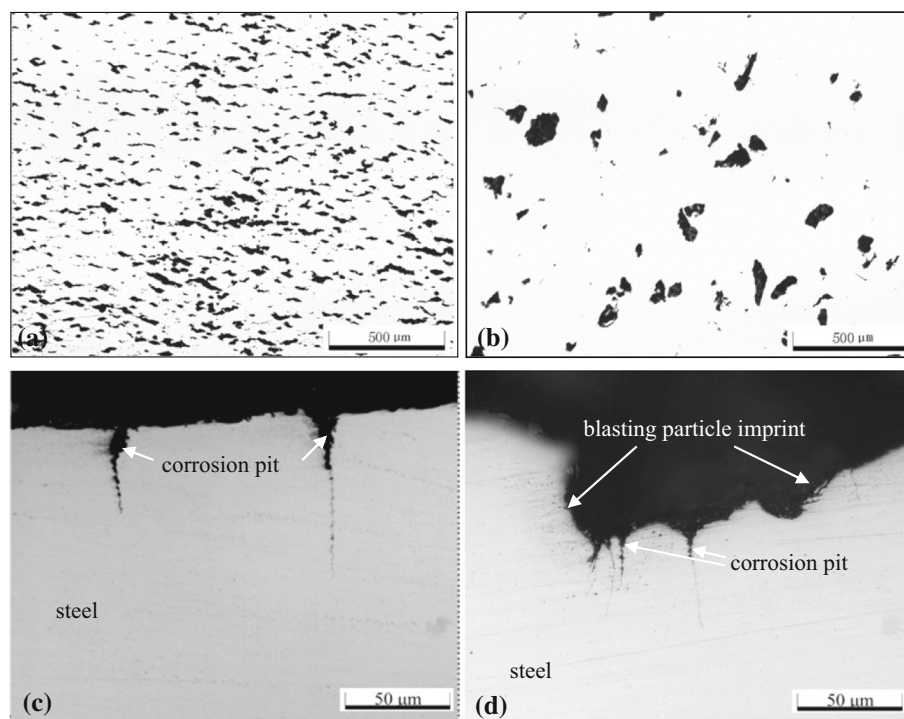
Fig. 10 Surface and cross-section morphology of corrosion fatigue specimen (333 MPa). (a) Bare steel, corrosion pits; (b) Steel substrate after coating removal, corrosion pits; (c) Bare steel, crack initiation sites; (d) Steel substrate after coating removal, crack initiation sites
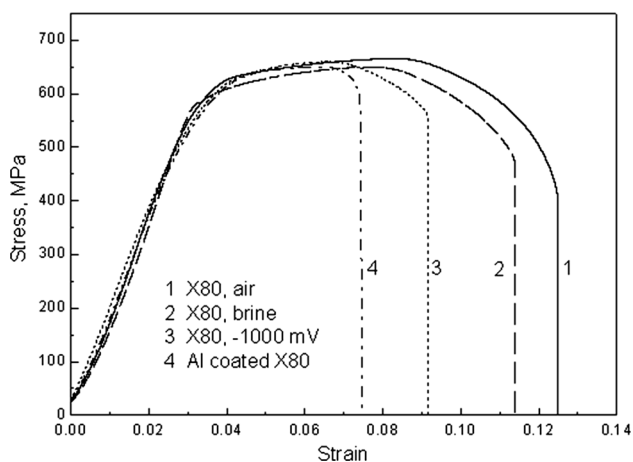

Fig. 11 Stress-strain curves of X80 and aluminum-coated X80

corrosion with the increase in roughness (Ref 26). Therefore, corrosion pits are formed in sandblast particle imprints, and then cracks are initiated from these corrosion pits after the aluminum coating loses its effective protection.

4.2 Crack Propagation Mechanism

The crack propagation of X80 under corrosion fatigue may be determined by anodic dissolution induced by local strain and/or environmental HE, but a previous study (Ref 27) showed that anodic dissolution was not the main cause

of corrosion fatigue crack propagation of X80 in 3.5 wt.% NaCl. Thus, HE controls the crack propagation process. SSRT can be used to study the sensitivity of materials to HE. Figure 11 shows the SSRT results for bare steel (under self-corrosion and -1000 mV) and aluminum-coated steel (under self-corrosion). The breaking elongation of X80 under self-corrosion state is evidently high, but thermally sprayed aluminum coating can markedly reduce the elongation rate of the steel substrate. In addition, the degree of decrease is greater than that with the application of impressed current cathodic protection at -1000 mV.

To quantify environmental embrittlement, it is classical to define a factor of embrittlement F based on the respective reduction of area observed under corrosive environment or under air as written in the following equation (Ref 28):

$$F = (RA_a - RA_e)/RA_a \times 100\% \qquad (Eq\ 6)$$

In which RA is the average reduction of area of the specimen tested under air or under corrosive environment. Reduction of area in Eq 6 can be replaced by other parameters, such as time to failure and plastic elongation. Fracture-absorbed energy, which is the envelope area under the stress-strain curve, reveals the combined influence of plastic elongation, breaking stress and time to failure. Therefore, fracture energy E was used to replace RA in Eq 6.

With this definition, brittleness index $F = 0$ means no environmental embrittlement whereas $F = 100\%$ means complete loss of ductility. Figure 12 shows the brittleness index of X80 steel (under self-corrosion and -1000 mV
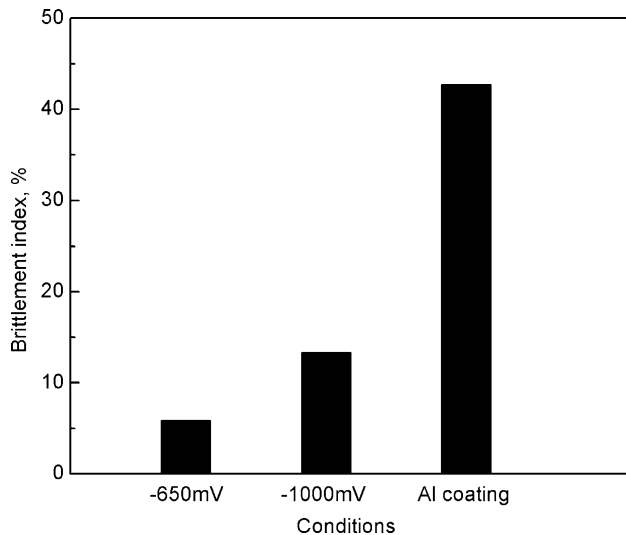
Fig. 12 Brittleness index under different conditions

polarization conditions) and aluminum-coated steel. The sensitivity to brittleness increases with the increase in brittleness index. Similar to that with -1000 mV polarization, aluminum coating could cause evident increase in brittleness, and the brittleness index of aluminum-coated X80 steel is higher than 40%, which shows apparent brittle characteristics. Inappropriate impressed current cathodic protection can cause hydrogen permeation into steel, leading to HE, and thus, the aluminum coating could also induce cathodic over-protection. Considering the effect of aluminum coating on the fatigue crack growth rate of X80 steel (Fig. 7), the cathodic protection function of aluminum coating could cause local HE at the tip of a crack, which can be attributed to the higher crack growth rate of aluminum-coated steel than that of bare steel.

The cathodic protection function of aluminum coating accelerates crack propagation, but this function also inhibits corrosion and induces a corrosion fatigue behavior of aluminum-coated steel in 3.5 wt.% NaCl that is similar to that of steel in air. The crack initiation stage was remarkably extended, whereas the percentage of crack propagation stage in the total fatigue life was significantly decreased. Therefore, the corrosion fatigue life of aluminum-coated steel is considerably longer than that of bare steel.

5. Conclusion

(1) Aluminum coating could significantly improve the corrosion fatigue life of steel substrates, and this influence would be enhanced by decreasing applied stress. However, the crack growth rate of aluminum-coated X80 steel was slightly higher than that of bare X80 steel.

(2) The mechanical isolation function and cathodic protection function made the aluminum coating influence the crack initiation stage of steel substrate. The total stress level in surface layer of steel substrate affects the mechanical isolation function of coating, thus influence the relative fatigue life of fatigue life. Cathodic protection function inhibits the corrosion of sandblast particle imprints, which further hinders crack initiation.

(3) Aluminum coating could cause local HE at the tip of a crack, which causes the relatively high crack growth rate of aluminum-coated steel compared with that of bare steel. The inhibiting effect of aluminum coating on crack initiation outweighs its promotion of crack propagation. Thus, the corrosion fatigue life of aluminum-coated steel is markedly longer than that of bare steel.

Acknowledgments

References

1. Y. Bai and Q. Bai, *Subsea Pipelines and Risers*, Elsevier, Oxford, 2005
2. W. Zhao, Y. Wang, T. Zhang, and Y. Wang, Study on the Mechanism of High-Cycle Corrosion Fatigue Crack Initiation in X80 Steel, *Corros. Sci.*, 2012, **57**, p 99-103
3. R. Pérez-Mora, T. Palin-Luc, C. Bathias, and P.C. Paris, Very High Cycle Fatigue of a High Strength Steel Under Sea Water Corrosion: A Strong Corrosion and Mechanical Damage Coupling, *Int. J. Fatigue*, 2015, **74**, p 156-165
4. R. Wang, *Corrosion Fatigue of Metallic Materials*, Northwestern Polytechnical University Press, Xi'an, 2001
5. F. Ahnia and B. Demri, Evaluation of Aluminum Coatings in Simulated Marine Environment, *Surf. Coat. Technol.*, 2013, **220**, p 232-236
6. J.A. Ellor, W.T. Young, and J. Repp, Thermally Sprayed Metal Coatings to Protect Steel Pilings: Final Report and Guide, Transportation Research Board, 2004
7. K.P. Fischer, W.H. Thomason, T. Rosbrook, and J. Murali, Performance History of Thermal-Sprayed Aluminum Coatings in Offshore Service, *Mater. Perform.*, 1995, **34**, p 27-35
8. S. Kuroda, J. Kawakita, M. Komatsu, T. Aoyagi, and H. Saitoh, Characterization of Thermal Sprayed Zn and Al Coatings after 18 Years Exposure in Marine Environment, *Meeting Abstracts, The Electrochemical Society*, 2006, p. 281
9. W.-M. Zhao, Y. Wang, C. Liu, L.-X. Dong, H.-H. Yu, and H. Ai, Erosion–Corrosion of Thermally Sprayed Coatings in Simulated Splash Zone, *Surf. Coat. Technol.*, 2010, **205**, p 2267-2272
10. Y. Horng, T. Chang, J. Hsu, and H. Shih, The Erosive Wear and Corrosion Behavior Of Zinc- and Aluminum-Coated Steels in Simulated Coastal Environment, *Surf. Coat. Technol.*, 2003, **168**, p 209-215
11. R. Ramanauskas, L. Gudaviciute, L. Diaz-Ballote, P. Bartolo-Perez, and P. Quintana, Corrosion Behaviour of Chromated Zn and Zn Alloy Electrodeposits, *Surf. Coat. Technol.*, 2001, **140**, p 109-115
12. K. Liu, P. Ma, N. Pu, J. Chen, and Q. Han, Influence of Silicon Coating on the Corrosion Resistance of Zn-Al-Mg-RE-Si Alloy, *J. Rare Earths*, 2010, **28**, p 378-381

13. R.A. Khan, A. Kaur, S. Singh, and S. Ahmad, Nonlinear Dynamic Analysis of Marine Risers Under Random Loads for Deepwater Fields in Indian Offshore, *Procedia Eng.*, 2011, **14**, p 1334-1342

14. X. Liu, G. Chen, Y. Chang, K. Liu, L. Zhang, and L. Xu, Analyses and Countermeasures of Deepwater Drilling Riser Grounding Accidents Under Typhoon Conditions, *Pet. Explor. Dev.*, 2013, **40**, p 791-795

15. G. Zhang, M. Gong, Q. Tang, T. Zhang, and X. Zeng, Electrochemical Study on Cathodic Protection Parameters of X80 Pipeline Steels, *Corros Prot.*, 2011, **32**, p 868-871

16. F. Zucchi, V. Grassi, C. Monticelli, and G. Trabanelli, Hydrogen Embrittlement of Duplex Stainless Steel Under Cathodic Protection in Acidic Artificial Sea Water in the Presence of Sulphide Ions, *Corros. Sci.*, 2006, **48**, p 522-530

17. D. Figueroa and M. Robinson, The Effects of Sacrificial Coatings on Hydrogen Embrittlement and Re-embrittlement of Ultra High Strength Steels, *Corros. Sci.*, 2008, **50**, p 1066-1079

18. X. Tang, Hydrogen Permeation Behavior of Hot-Dipped Steel in Seawater and Its Effects on the Mechanical Properties of Steel Substrate. The Chinese Academy of Sciences 2006

19. R.T.R. McGrann, D.J. Greving, J.R. Shadley, E.F. Rybicki, T.L. Kruecke, and B.E. Bodger, The Effect of Coating Residual Stress on the Fatigue Life of Thermal Spray-Coated Steel and Aluminum, *Surf. Coat. Technol.*, 1998, **108-109**, p 59-64

20. P. Paris and F. Erdogan, A Critical Analysis of Crack Propagation Laws, *J. Basic Eng.*, 1963, **85**, p 528-533

21. M. Multigner, S. Ferreira-Barragáns, E. Frutos, M. Jaafar, J. Ibáñez, P. Marín, M.T. Pérez-Prado, G. González-Doncel, A. Asenjo, and J.L. González-Carrasco, Superficial Severe Plastic Deformation of 316 LVM Stainless Steel Through Grit Blasting: Effects on Its Microstructure and Subsurface Mechanical Properties, *Surf. Coat. Technol.*, 2010, **205**, p 1830-1837

22. E.M. Gutman, *Mechanochemistry and Corrosion Prevention of Metals*, Science Publication, Peking, 1989

23. S. Barriuso, J. Chao, J. Jiménez, S. García, and J. González-Carrasco, Fatigue Behavior of Ti6Al4V and 316 LVM Blasted with Ceramic Particles of Interest for Medical Devices, *J. Mech. Behav. Biomed. Mater.*, 2014, **30**, p 30-40

24. E.S. Puchi-Cabrera, M.H. Staia, Y.Y. Santana, E.J. Mora-Zorrilla, J. Lesage, D. Chicot, J.G. La Barbera-Sosa, E. Ochoa-Perez, and C.J. Villalobos-Gutierrez, Fatigue Behavior of AA7075-T6 Aluminum Alloy Coated with a WC–10Co–4Cr Cermet by HVOF Thermal Spray, *Surf. Coat. Technol.*, 2013, **220**, p 122-130

25. E.S. Puchi-Cabrera, M.H. Staia, M.J. Ortiz-Mancilla, J.G. La Barbera-Sosa, E.A.O. Pérez, C. Villalobos-Gutiérrez, S. Bellayer, M. Traisnel, D. Chicot, and J. Lesage, Fatigue Behavior of a SAE 1045 Steel Coated with Colmonoy 88 Alloy Deposited by HVOF Thermal Spray, *Surf. Coat. Technol.*, 2010, **205**, p 1119-1126

26. V. Barranco, E. Onofre, M. Escudero, and M. Garcia-Alonso, Characterization of Roughness and Pitting Corrosion of Surfaces Modified by Blasting and Thermal Oxidation, *Surf. Coat. Technol.*, 2010, **204**, p 3783-3793

27. W. Zhao, R. Xin, Z. He, and Y. Wang, Contribution of Anodic Dissolution to the Corrosion Fatigue Crack Propagation of X80 Steel in 3.5 wt.% NaCl Solution, *Corros. Sci.*, 2012, **63**, p 387-392

28. L. Briottet, R. Batisse, G. de Dinechin, P. Langlois, and L. Thiers, Recommendations on X80 steel for the Design of Hydrogen Gas Transmission Pipelines, *Int. J. Hydrogen Energy*, 2012, **37**, p 9423-9430